Technological University Dublin

ARROW@TU Dublin

Articles

School of Electrical and Electronic Engineering

2011-10-01

Numerical Study of an Ion-Exchanged Glass Waveguide Using Both Two-Dimensional and Three-Dimensional Models

Pengfei Wang
Technological University Dublin, pengfei.wang@tudublin.ie

Yuliya Semenova
Technological University Dublin, yuliya.semenova@tudublin.ie

Jie Zheng
Jilin University

Qiang Wu
Technological University Dublin, qiang.wu@tudublin.ie

Agus Hatta
Technological University Dublin, ahatta@tudublin.ie
Follow this and additional works at: https://arrow.tudublin.ie/engscheceart

Part of the Engineering Commons
See next page for additional authors

Recommended Citation

Authors

Pengfei Wang, Yuliya Semenova, Jie Zheng, Qiang Wu, Agus Hatta, and Gerald Farrell

Numerical study of an ion-exchanged glass waveguide using both two-dimensional and three-dimensional models

Pengfei Wang[1,] Yuliya Semenova[1], Jie Zheng[2], Qiang Wu[1], Agus Muhamad Hatta[1] and Gerald Farrell[1]

[1]Photonics Research Center, School of Electronic and Communications Engineering, Dublin Institute of Technology, Kevin Street, Dublin 8, Ireland;

[2]State Key Laboratory of Integrated Optoelectronics, College of Electronic Science and Engineering, Jilin University, Changchun 130012, P. R. China

E-mail: pengfei.wang@dit.ie

Abstract: A numerical study is carried out to compare the two-dimensional (2-D) case and three-dimensional (3-D) case for the modelling of an ion-exchanged glass waveguide. It is shown that different waveguide widths on the photomask correspond to different ion concentration distributions after an annealing process. A numerical example is presented of two waveguide sections with different widths indicates that due to the abrupt change of the waveguide width, a 3-D theoretical model is required for an accurate prediction of the parameters of ion-exchanged glass waveguides. The good agreement between the modelled and measured results proves that the developed 3-D numerical model can be beneficially utilized in the generalized design of optical devices based on ion-exchange waveguides.

Keywords: Integrated optics device, glass waveguide, ion exchange, annealing

1. Introduction

Ion-exchanged glass waveguides have been investigated extensively for applications in the area of integrated optics due to their superior characteristics such as low-propagation loss and the relatively simple fabrication technique involved. An ion-exchanged glass waveguide has a graded index profile which distinguishes it from a waveguide with a step-index profile, such as a silica-on-silicon buried waveguide, a polymer waveguide or a silicon-on-insulator waveguide. Defining the index profile is

an important preliminary step in the simulation and design of planar lightwave circuits. For ion-exchanged glass waveguides one commonly used method is based on an approximation of the refractive index profile by a semi-Gaussian function in the horizontal direction (parallel to the glass surface) and by a complementary error function in the vertical direction, which requires the so-called diffusion depth parameters d_x and d_y to be estimated experimentally [1-4]. This simulation method works well for some simple ion-exchanged integrated circuits devices, such as channel or tapered waveguides. However, for more complex optical devices, such as a buried waveguide and an array-waveguide grating multiplexer, simulations based on the ion diffusion equation model are more desirable since the semi-Gaussian function has a limited accuracy.

It is known that a during fabrication the desired refractive index profile is achieved by control of the experimental parameters: ion-exchange time, annealing time, temperature and the waveguide widths defined by the photomask layout. Using initial values of these parameters, it is possible to derive the ion-concentration distribution [5-11] and hence the refractive index profile can be found by solving the diffusion equation numerically. Using the calculated refractive index profile, a simulation can be carried out to determine the optical performance of the device. Based on this simulation further iterations of process above can be carried until the desired optical performance is achieved and with it a knowledge of correct values of the experimental parameters needed. Therefore, in this paper modelling of the refractive index profile of an ion-exchanged glass waveguide through numerical calculation of the diffusion equation is considered.

In practice, integrated optical components based on planar lightwave circuits usually consist of waveguide sections with different widths. Ref. [10] presented an investigation of the dependence of burial-depth on waveguide width for a buried ion-exchanged glass waveguide. In this paper, the influence of the waveguide width of the photomask on the ion concentration distribution is investigated for ion-exchanged glass waveguides based on thermal ion-exchange and annealing. Both 2-D and 3-D models are presented. The results for the 2-D modelling indicate that for the ion-exchanged waveguide, different waveguide widths result in a significantly different distribution for the ion concentration after annealing. For ion-exchanged waveguide

devices that require an abrupt change in the waveguide width, for example a multimode interference based coupler or an arrayed-waveguide grating, a 3-D model is presented. A numerical example of a structure consisting of two waveguide sections with different widths is presented. Through comparison between the simulation results obtained with the 2-D and 3-D models, it is found that for the case of an abrupt change of the waveguide width, a 3-D model is necessary to ensure an accurate prediction of the ion concentration in the transition region near the interface. Additionally the mode patterns for an ion-exchanged waveguide based multimode interferometer (MMI) are investigated and presented. The investigation involves both theoretical modeling and experimental verification. The 3-D numerical model shows a good agreement with the measured mode pattern results for the ion-exchanged optical devices.

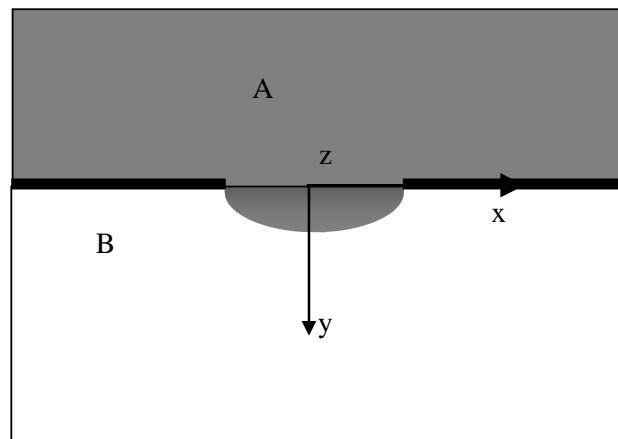## 2. Modelling of an ion-exchange process for the 2-D case

Fig. 1 Schematic diagram of the ion-exchange process.

Fig.1 presents a schematic diagram of the ion-exchange process without an applied voltage. The nonlinear diffusion equation for ion-exchange is [5-11]

$$\frac{\partial}{\partial t}C = \frac{D_A}{1-\alpha C}\left[\nabla^2 C + \frac{\alpha}{1-\alpha C}(\nabla C)^2\right] \qquad (1)$$
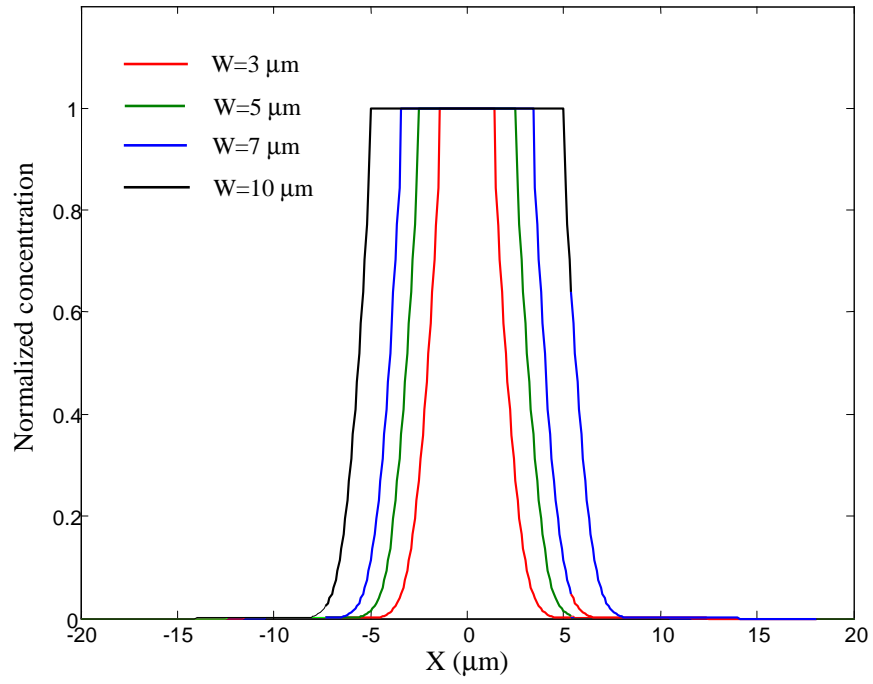
where C is the normalized ion concentration of A ions. $\alpha = 1 - D_A/D_B$, D_A and D_B are the self-diffusion coefficients for A ions and B ions respectively. This non-linear

equation has no analytical solutions and therefore some numerical algorithms have been used in previous investigations, such as the explicit Dufort-Frankel method [12] and the method of Peaceman and Rachford (PR-ADI) [13]. Our numerical calculation indicates that both methods can produce similar simulation results but the explicit Dufort-Frankel method is computationally faster. For the same computer hardware specifications the calculation time for the explicit Dufort-Frankel method can be reduced to less than a half of the calculation time needed with the other two methods. Furthermore, this method can be easily expanded for a 3-D case. Therefore, the explicit Dufort-Frankel method is used in this paper.

When the waveguide is uniform in the z-direction, i.e., $\dfrac{\partial}{\partial z} = 0$, a 2-D model can be used. Denoting $f_1 = \dfrac{D_A}{1 - \alpha C_{i,j}^n}$ and $f_2 = f_1 \dfrac{\alpha}{\left(1 - \alpha C_{i,j}^n\right)}$ then the 2-D diffusion equation has the form:

$$\left[1 + \frac{2\Delta t f_1}{\Delta x^2} + \frac{2\Delta t f_1}{\Delta y^2}\right]C_{i,j}^{n+1} = \left[1 - \frac{2\Delta t f_1}{\Delta x^2} - \frac{2\Delta t f_1}{\Delta y^2}\right]C_{i,j}^{n-1} + \frac{2\Delta t f_1}{\Delta x^2}\left[C_{i,j+1}^n + C_{i,j-1}^n\right]$$
$$+ \frac{2\Delta t f_2}{4\Delta x^2}\left[C_{i,j+1}^n - C_{i,j-1}^n\right]^2 + \frac{2\Delta t f_1}{\Delta y^2}\left[C_{i+1,j}^n + C_{i-1,j}^n\right] + \frac{2\Delta t f_2}{4\Delta y^2}\left[C_{i+1,j}^n - C_{i-1,j}^n\right]^2 \tag{2}$$

The corresponding boundary condition can be found from Ref. [5]. To consider the influence of the waveguide width on the refractive index profile, a numerical example of an Ag^+-Na^+ ion-exchange process is presented. From Ref. [6] $D_A = 5.1 \times 10^{-6}$ and $\alpha = 0.87$. The ion-exchange and annealing times are 20 and 35 minutes, respectively. Waveguide widths of 3, 5, 7 and 10 μm on the photomask are considered. The simulation results for the ion concentration distribution are presented in Fig.2a and Fig.2b.

(a)
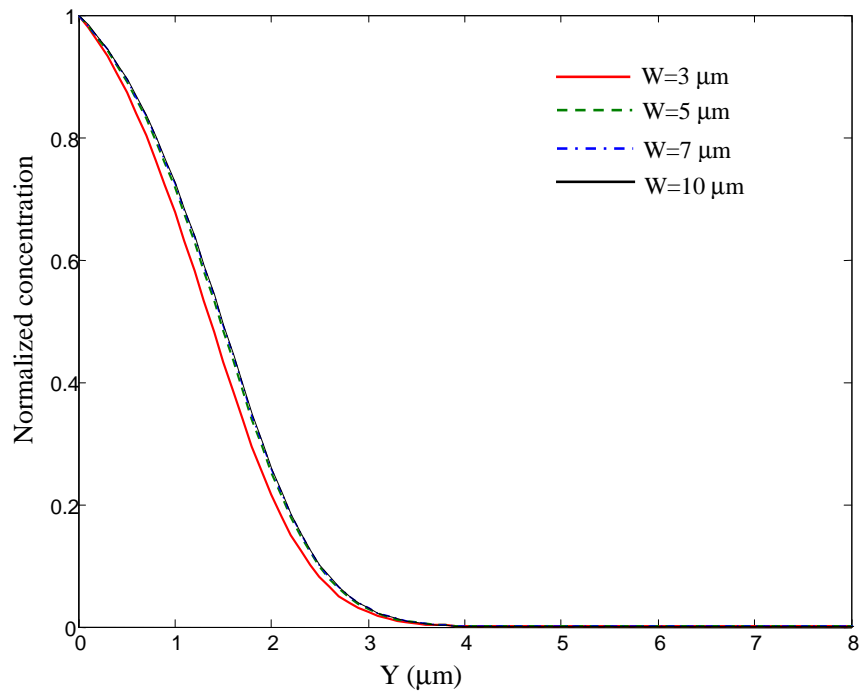
(b)

Fig. 2 Normalized distributions of the ion concentration after thermal ion-exchange in (a) x-direction; (b) y-direction.

Fig. 2a presents the normalized ion concentrations in the x-direction parallel to the glass surface and Fig. 2b presents the normalized ion concentration in the y-direction in the middle of the waveguide. It can be seen that in the y-direction, there is no apparent difference between the ion concentration distributions for different waveguide widths. Thermal annealing is usually carried out after ion-exchange, which has been shown [14] to improve the fiber coupling efficiency and decrease the propagation loss. The calculated ion concentration distributions after the thermal annealing process are presented in Fig. 3a and Fig. 3b.
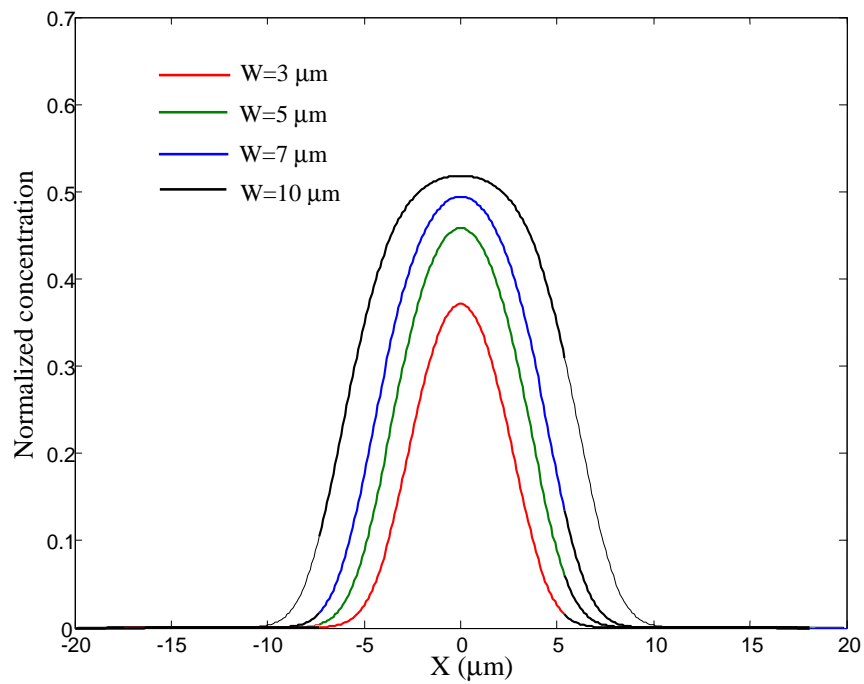
(a)
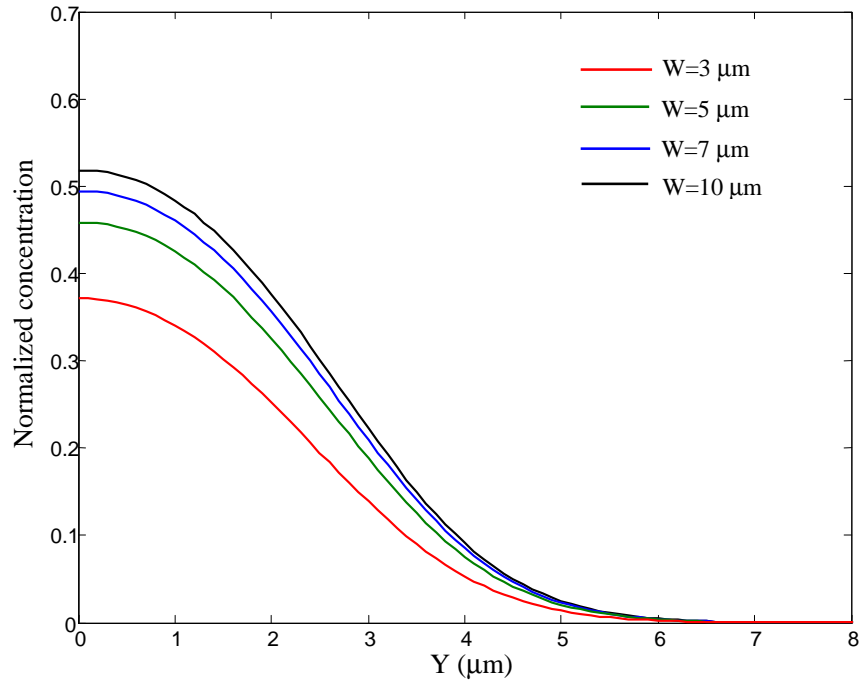
(b)

Fig. 3 Normalized ion concentration distributions after the thermal annealing process in (a) x-direction; (b) y-direction.

Fig. 3 shows that after thermal annealing, the ion concentration profiles differ significantly for different waveguide widths, including the amplitude of the maximum concentration. This numerical example shows that different waveguide widths correspond to significantly different ion concentration profiles. This 2-D model is suitable for a waveguide with a uniform width or a slowly varying tapered waveguide in the z-direction. However, the 2-D model presented above cannot predict the ion concentration distributions in the case of an abrupt change of the waveguide width, for example the transition region of a multimode interferometer, therefore a 3-D model is required for prediction in such an integrated device fabricated through the ion-exchange or diffusion process.

3. Modelling of an ion-exchange process with a 3-D model

Similar to the 2-D model, with the explicit Dufort-Frankel method, the diffusion equation for the 3-D case is:

7

$$\left[1+\frac{2\Delta tf_1}{\Delta x^2}+\frac{2\Delta tf_1}{\Delta y^2}+\frac{2\Delta tf_1}{\Delta z^2}\right]C_{i,j,k}^{n+1}=\left[1-\frac{2\Delta tf_1}{\Delta x^2}-\frac{2\Delta tf_1}{\Delta y^2}-\frac{2\Delta tf_1}{\Delta z^2}\right]C_{i,j,k}^{n-1}+$$

$$\frac{2\Delta tf_1}{\Delta x^2}\left[C_{i,j+1,k}^{n}+C_{i,j-1,k}^{n}\right]+\frac{2\Delta tf_2}{4\Delta x^2}\left[C_{i,j+1,k}^{n}-C_{i,j-1,k}^{n}\right]^2+\frac{2\Delta tf_1}{\Delta y^2}\left[C_{i+1,j,k}^{n}+C_{i-1,j,k}^{n}\right] \quad (3)$$

$$+\frac{2\Delta tf_2}{4\Delta y^2}\left[C_{i+1,j,k}^{n}-C_{i-1,j,k}^{n}\right]^2+\frac{2\Delta tf_1}{\Delta z^2}\left[C_{i,j,k+1}^{n}+C_{i,j,k-1}^{n}\right]+\frac{2\Delta tf_2}{4\Delta z^2}\left[C_{i,j,k+1}^{n}-C_{i,j,k-1}^{n}\right]^2$$

Consider a structure consisting of two waveguide sections (section I and section II) with a different waveguide widths of w_0 and w_1 as shown in Fig.4. In practice such a structure corresponds to the entry section of an MMI device. For the numerical calculation it is assumed that $w_0 = 3\mu m$ and $w_1 = 15\mu m$. The area of the calculation region is 40×200 μm^2 in the x-z plane and the interface between the two waveguide sections lies at $z = 100\mu m$.
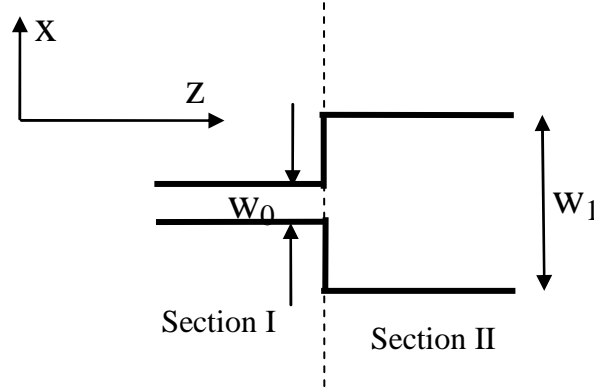

Fig. 4 Schematic structure of a two-waveguide section with the widths w_0 and w_1.

Using the same experimental parameters as the 2-D case, with the three-dimensional model, the ion concentration profile in the x-z plane at the surface of the glass is presented in Fig. 5. From Fig. 5, the interface between the two waveguide sections can be clearly seen. The corresponding ion-concentration distributions in the x-direction and y-direction are plotted in Fig. 6a and Fig. 6b. The calculated results with the 2-D model are also presented in Fig. 6a and Fig. 6b. The 2-D model results were obtained by considering the waveguide sections I and II independently. It can be seen that the ion concentration near the interface is different from the profile for widths of 3 μm and 15 μm. From the calculated results one can see that at the

interface and in the region around the interface in waveguide section I, the ion concentration obtained by the 3-D model has a different distribution by comparison with the results obtained from the 2-D case. For the ion concentration distribution in the y-direction, there is no apparent difference for different waveguide sections. However, in Fig. 6 (a) and (b), one can also see that in the transition region of the proposed multimode interferometer, that is $95\mu m \leq Z \leq 100\mu m$ along the propagation direction, the 2-D model presented in Sec. 2 cannot calculate the distribution of ion concentration for both x and y-direction cases.
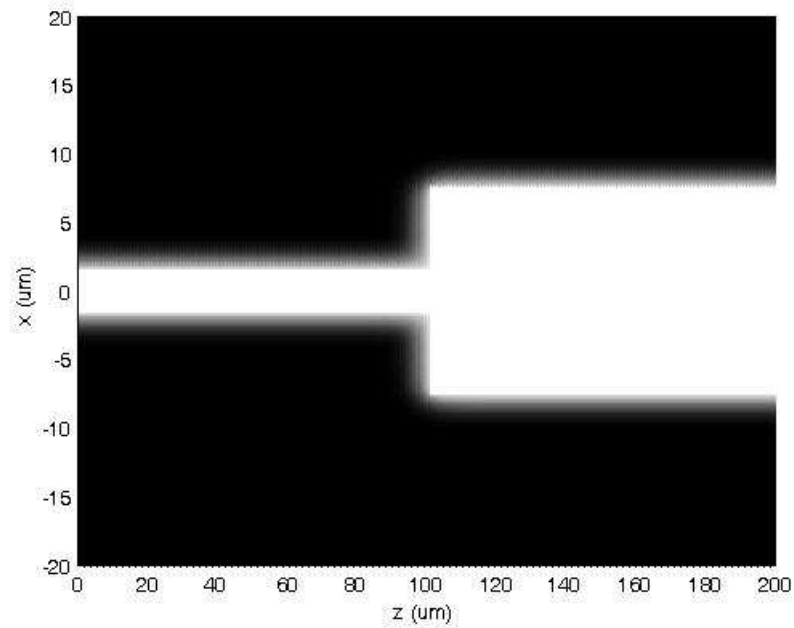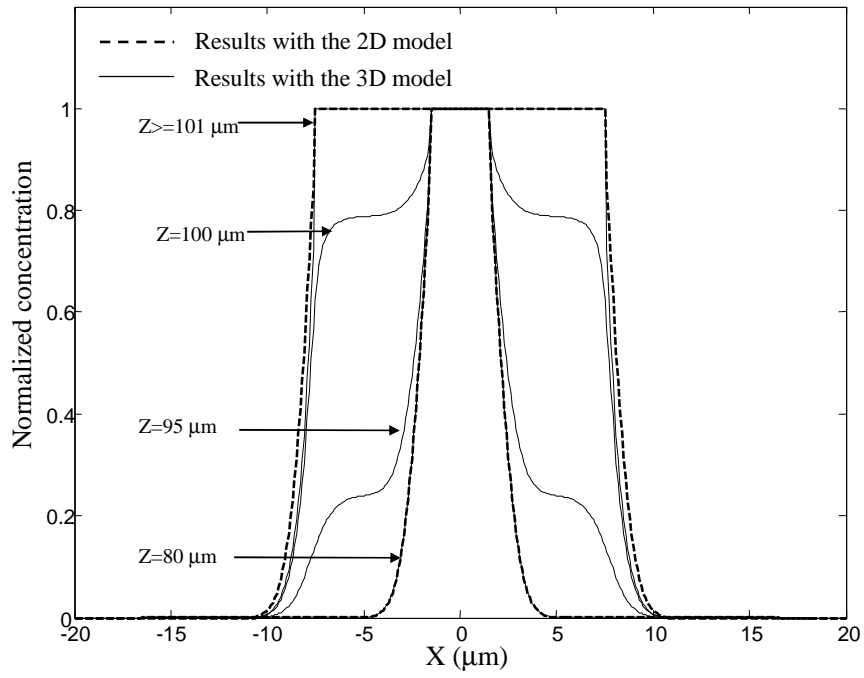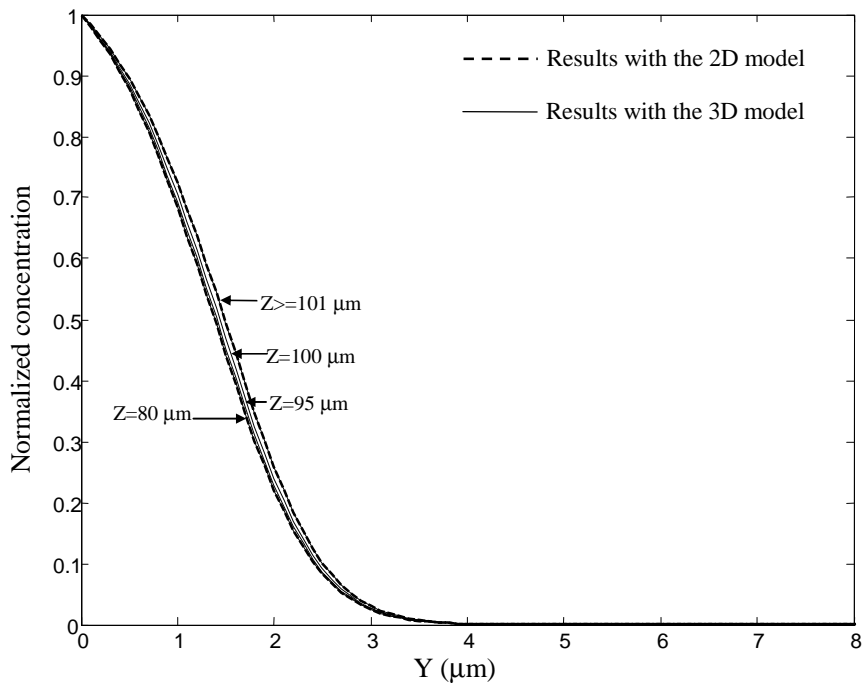

Fig. 5 Ion concentration profile in the x-z plane at the surface of glass.

9

(a)

(b)

Fig.6 Normalized ion concentration distributions after the thermal ion-exchange process for the structure in Fig. 4 in (a) x-direction; (b) y-direction.

The calculated ion concentration distribution in the x-z plane at the surface of glass after 35 minutes of thermal annealing is presented in Fig.7. It can be seen that the waveguide boundaries are not as clear as in the distribution presented in Fig. 5, and the transition region between singlemode and multimode waveguides is extended. The corresponding ion-concentrations in the x-direction and y-direction at different z-coordinates are plotted in Fig.8a and Fig.8b.
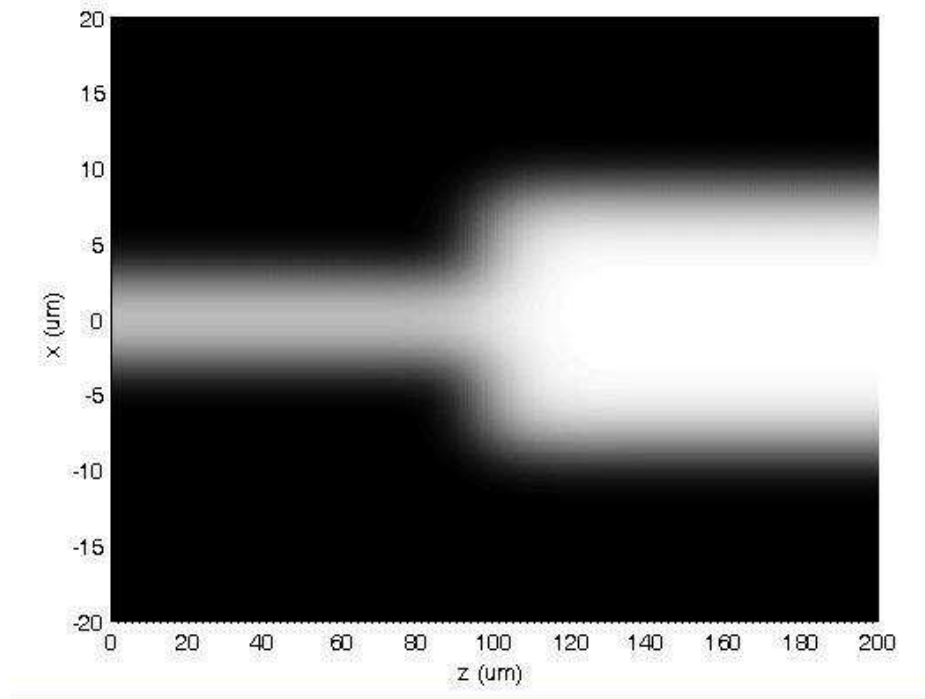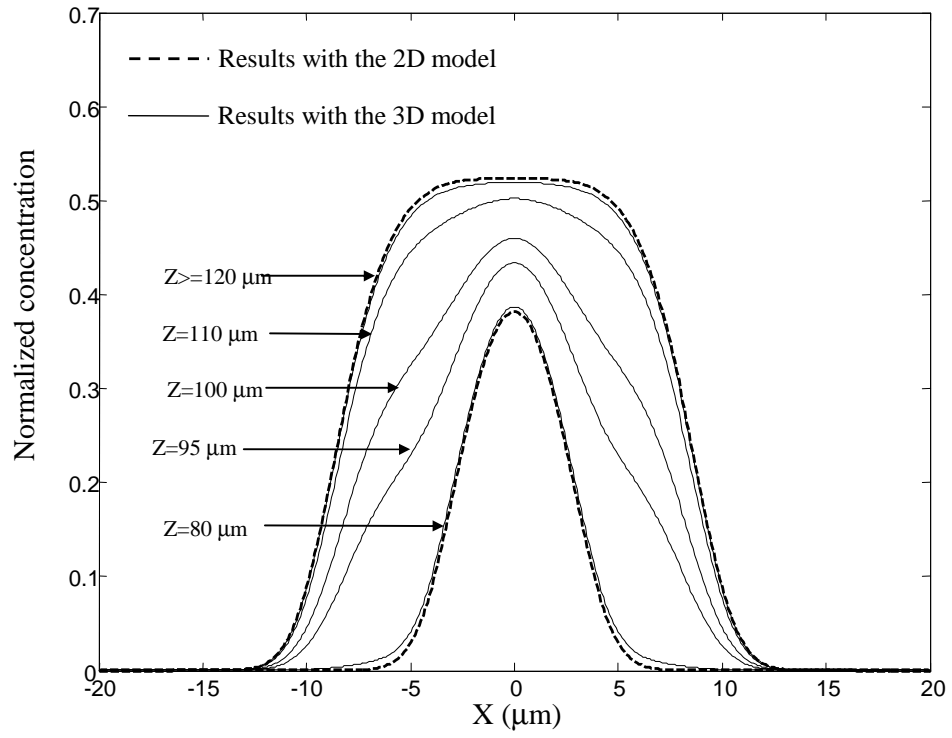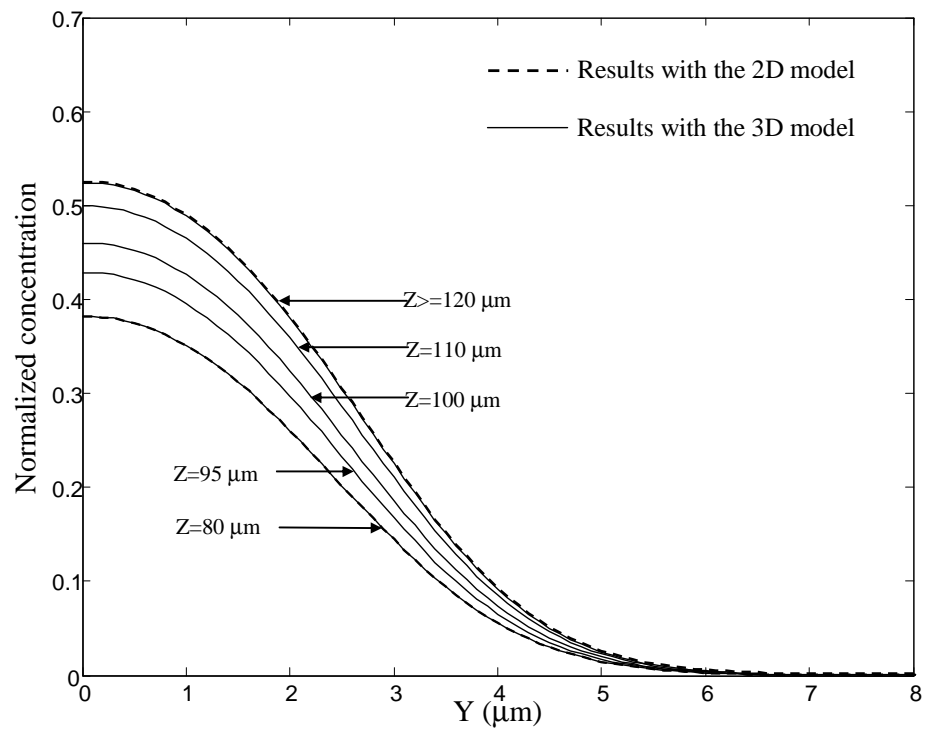

Fig. 7 Ion concentration profile in the x-z plane at the surface of the glass after annealing.

(a)

(b)

Fig. 8 Normalized ion concentration distributions after the thermal annealing process for
the structure in Fig. 4 in (a) x-direction; (b) y-direction.

From the modelling results presented in Fig. 8, it can be seen that distributions of the ion concentration are significantly different from the corresponding results presented in Fig. 6. In Fig. 6, the ion-concentration in the waveguide region II is identical to the results obtained by the 2-D model, but in Fig. 8a, one can see that only when $z \geq 120$ μm, does the distribution of ion concentration agree with that obtained by the 2-D model. From this example, one can see the significant influence of the abrupt change of the waveguide width on the corresponding index profile and if the 2-D model is used, the distribution of ion-concentration around the interface between the two waveguide sections cannot be obtained. The transition region between singlemode and multimode waveguides is extended from 5 μm (see Fig. 6 (a) & (b)) to 15 μm at least due to the annealing process which results in ion diffusion. This suggests that the 3-D model developed is essential for the accurate prediction for an ion-exchanged waveguide which undergoes an annealing process.

4. Optical performance of the ion-exchanged device

To illustrate the optical performance of the ion-exchanged waveguide device with an abrupt change of waveguide width, a simulation using a 3-D beam propagation method is carried out based on the different index profiles obtained with both 2-D and 3-D models. The maximum change of refractive index due to the ion-exchange is assumed to be $\Delta n = 0.049$ and the refractive index of the substrate is 1.504 at a wavelength of 1.55 μm. The ion-exchange and annealing times are 20 and 35 minutes, respectively.

In the simulations presented earlier in this paper, the device length considered is 200 μm but in practice fabricating a 200 μm long device and subsequently polishing the end facets to achieve the required optical quality is very difficult. Hence a longer device length was required in practice, which in principle would mean that simulations carried out for a device length of 200 μm could not be readily compared with experimental results for the fabricated longer device. However in our simulations, it was found that periodic real images occur within the section of the multimode waveguide due to the well-known self-focusing principle for a graded index waveguide [15, 16]. It was found that the profile of the optical field distribution of the proposed MMI device in the x-y plane at a distance of 500 μm from the input facet is

13

the same as that at a distance of 5000 μm. Hence in practice a 5000 μm long device is fabricated with the waveguide width transition at a distance of 100 μm from the input facet. The longer device length allows the end facets to be easily polished to achieve the desired optical quality and to adjust the total length precisely to 5000 μm. Additionally the computation window in the simulation along the z-direction is extended from 200 μm to 500 μm. The simulation results are presented in Fig. 9a and Fig. 9b, respectively. The input light used in the theoretical models has a wavelength of 1550 nm. Comparing Fig. 9a and Fig. 9b, it is clear that the light propagation differs due to the different index profiles obtained by the 2-D and 3-D models. For example, in Fig. 9 (a), there is no change in the intensity profile in the region up to the 100 μm transition point between the singlemode and multimode waveguides obtained by the 2-D model, but in Fig. 9 (b), one can see that increasing attenuation occurs in the region up to the transition point.

The corresponding simulated mode patterns of the device at a length of 5000 μm are presented in Fig. 10a and Fig. 10b. The mode patterns have the same shape at 5000 μm as those at 500 μm. Fig. 10a is based on the index profile obtained by the 2-D model, and Fig. 10b is based on the index profile obtained by the 3-D model. Through comparison of Fig. 10a and Fig. 10b, it is found that there is a significant difference in the optical field intensity and mode pattern from the output port for the 2-D and 3-D models. This suggests that for a graded-index waveguide structure involving an abrupt change in the waveguide width, a 3-D model is required to accurately predict the optical performance of the device.
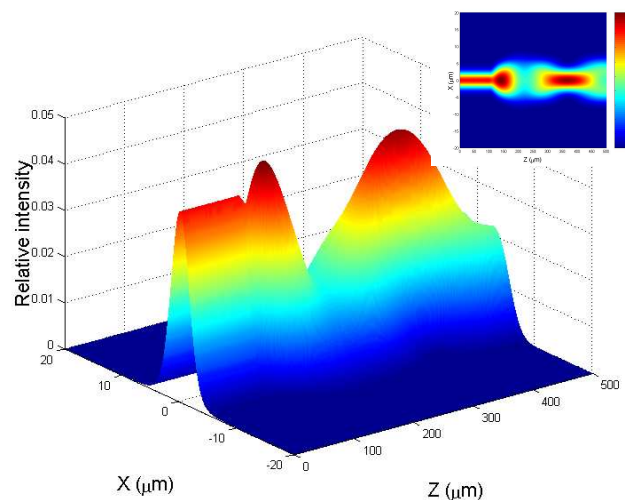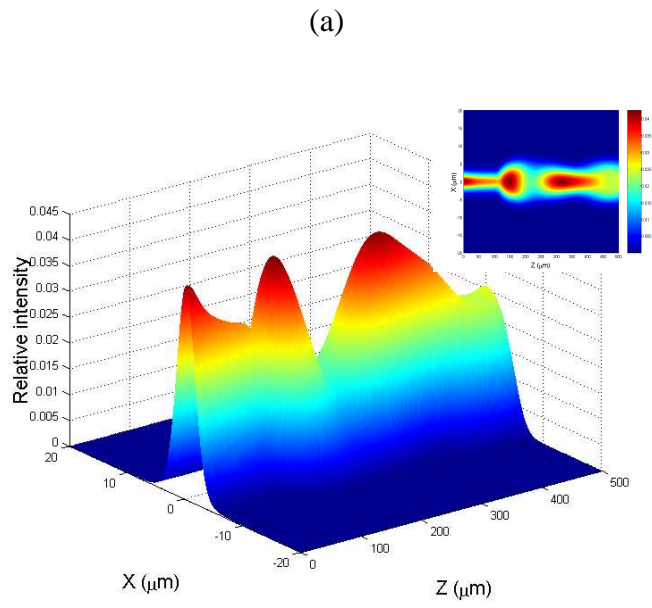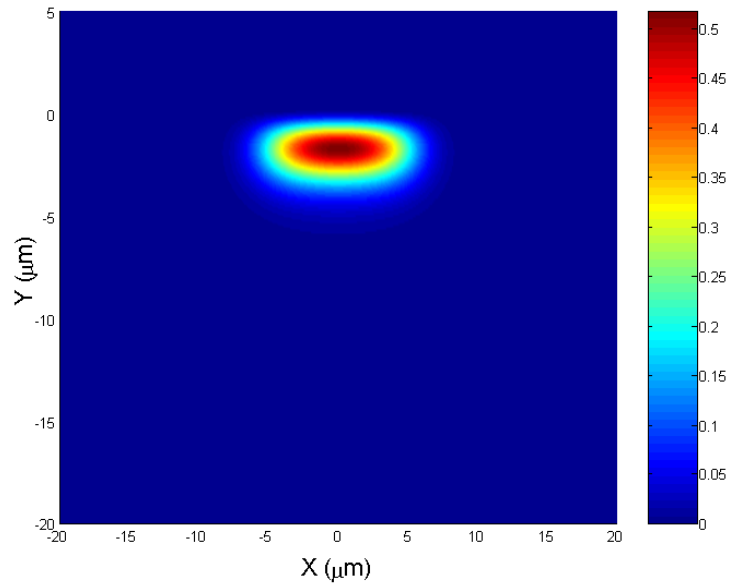
(b)

Fig.9 Light propagation in the x-z plane (both 2-D and 3-D plots) at the surface of the glass, based on the refractive index profile obtained by (a) 2-D model; (b) 3-D model.
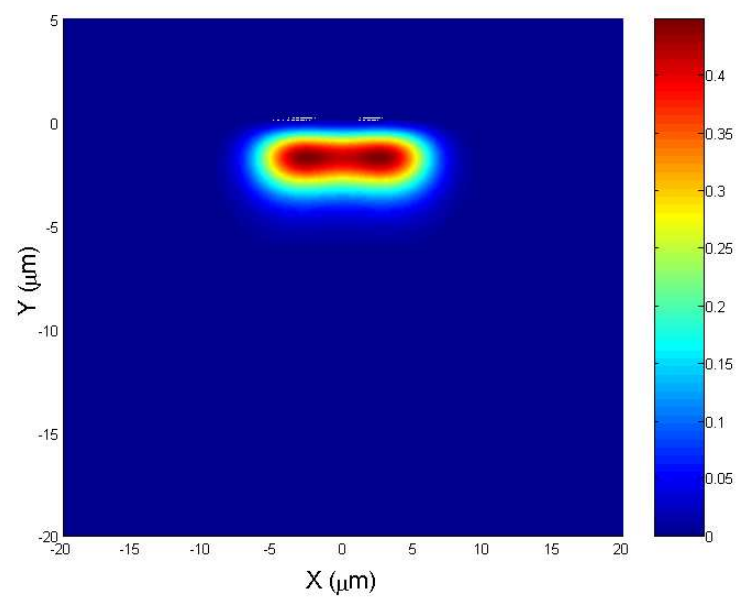
(a)

(b)

Fig.10. Optical field distribution in the x-y plane (cross-section view) based on the refractive index profile obtained by (a) 2-D model; (b) 3-D model.

5. Experimental evaluation

In order to verify the theoretical models for the ion-exchanged integrated device, the ion exchanged glass MMI device described earlier in this paper was fabricated. The chemical composition of the soda-lime glass used in the experiments is given in Table 1.

Table 1. Chemical composition of the soda-lime silicate glass employed in the experiments

Oxide	Weight (%)
SiO_2	73.15
Na_2O	14.35
CaO	8.20
Al_2O_3	0.25
K_2O	0.23
MgO	3.50
TiO_2	0.02
Fe_2O_3	0.15

In order to define the waveguide pattern on the soda-lime silicate glass, a 300-nm-thick aluminum film was deposited upon the pre-cleaned glass surface and standard photolithographic techniques were employed to define the openings in the film where ion-exchange could take place. The glass slides with the aluminum mask openings were immersed in an $AgNO_3$-$NaNO_3$ molten salt composition at a temperature of 330°C; the temperature was controlled and monitored by a digital temperature sensor. The process of ion-exchange of Ag^+ with the Na^+ in the glass slide was carried out for 20 minutes, after ion exchange, the glass sample was removed from the molten salt and the sample was then immediately washed in deionized water to remove residual surface salt. After the cleaning process, an annealing process followed at the same temperature for a period of 35 minutes. Finally, the entire glass device length was accurately set to a length of 5000 μm using end polishing and the aluminum mask was removed using acid.

As shown in Fig. 11, an experimental setup for measuring the mode patterns was built. The ion-exchanged device was mounted on a vacuum stage which was connected to a vacuum pump. A tunable laser is used as an optical source with an output power of 0 dBm at an operating wavelength of 1550 nm. At the waveguide end a microscope objective focuses the output light to an infrared camera which is controlled by a personal computer. A standard singlemode fiber with a tapered end is employed to connect the laser source and the sample, the fiber was aligned in X−Y direction until the measured transmitted optical power was maximised.
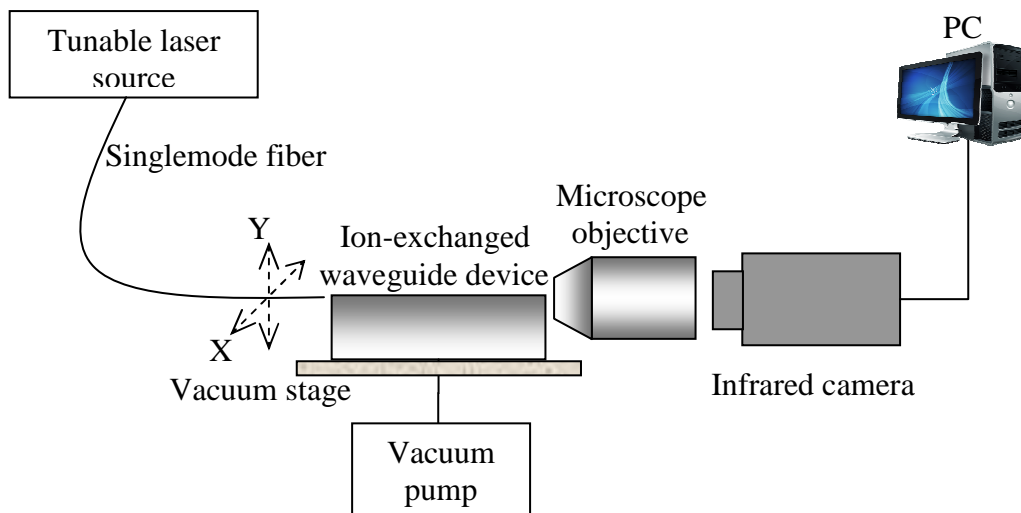
Fig. 11. Schematic representation of the ion-exchanged waveguide measurement setup

The setup in Figure 11 can be used to obtain the near field mode patterns of the waveguide end-facet. Figure 12 shows the end-facet mode pattern of the ion-exchanged MMI optical device at a wavelength of 1550 nm. From Fig. 10b and Fig. 12, one can see that there is a good agreement between the shape of mode pattern calculated using the 3-D theoretical model and the measured results.
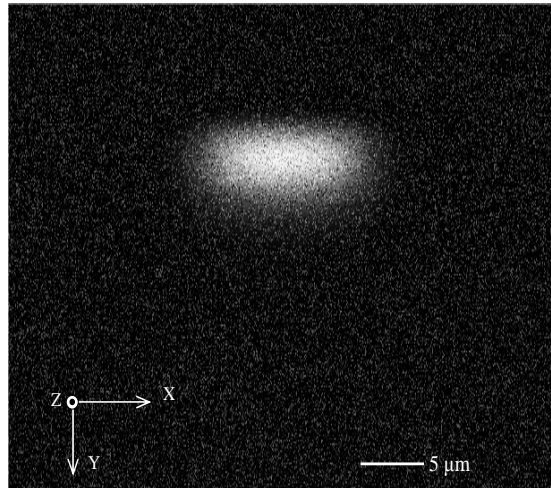

Fig. 12. Near-field mode pattern image of the ion-exchanged MMI device at the propagation direction of Z=5000 μm.

4. Conclusion

The modelling of an ion-exchanged glass waveguide has been investigated in this paper for both the 2-D and 3-D case. The 2-D model shows that different waveguide width on the photomask correspond to different ion concentration distributions after the annealing process. To illustrate the influence of the abrupt change of waveguide width on the distribution of the ion concentration, a comparison has been carried between the 2-D and 3-D models. A numerical example is presented based on two waveguide sections with different widths and is has been shown that due to the abrupt change of the waveguide width, a 3-D model is required for accurate modelling of such waveguide based devices. Furthermore, the agreement between the modelled and measured results also suggests that the 3-D theoretical numerical model developed can be beneficially utilized in the generalized design of ion-exchange waveguide based optical devices.

18

5. Acknowledgement

Reference

1. M. N. Weiss and R. Srivastava, "Determination of ion-exchanged channel waveguide profile parameters by mode-index measurements", App. Opt., Vol. 34, No. 3, pp.455-458, 1995.
2. S. J. Hettrick, J. I. Mackenzie, R.D. Harris, J. S. Wilkinson, D. P. Shepherd and A. C. Tropper, "Ion-exchanged tapered-waveguide laser in neodymium-doped BK7 glass", Opt. Lett., Vol. 25, No. 19, pp. 1433-1435, 2000.
3. A. Miliou, H. Zhenguang, H.C. Cheng, R. Srivastava, R. V. Ramaswamy, "Fiber-Compatible K^+-Na^+ Ion-Exchanged Channel Waveguides: Fabrication and characterization", IEEE J. Quantum Electron., Vol. 25, No. 8, pp. 1889-1897, 1989.
4. R. A. Betts, F. Lui and S. Dagias, "Wavelength and polarization insensitive optical splitters fabricated in K^+/Na^+ Ion-exchanged glass", IEEE Photon. Technol. Lett., Vol. 2, No. 7, pp.481-483, 1990.
5. B. R. West, P. Madasamy, N. Peyghambarian and S. Honkanen, "Modeling of ion-exchanged glass waveguide structures", J. Non-Crystalline Solids, Vol. 347, pp. 18-26, 2004.
6. J. T. A . Carriere, J. A. Frantz, B. R. West, S. Honkanen and R. K. Kostuk, "Bend loss effects in diffused, buried waveguides", App. Opt., Vol. 44, No. 9, pp. 1698-1703, 2005.
7. J. M. Castro, D. F. Geraghty, B. R. West and S. Honkanen, "Fabrication and comprehensive modelling of ion-exchanged Bragg optical add-drop multiplexers", App. Opt. Vol. 43, No. 33, pp. 6166-6173, 2004.

8. B. Buchold, C. Glingener, D. Culemann and E. Voges, "Polarization insensitive ion-exchanged array-waveguide grating multiplexers in glass", Fiber and Integrated Optics, Vol. 17, pp. 279-298, 1998.

9. S. Yliniemi, B. R. West and S. Honkanen, "Ion-exchanged glass waveguides with low birefringence for a broad range of waveguide widths", App. Opt., Vol. 44, No. 16, pp. 3358-3363, 2005.

10. P. Madasamy, B. R. West, M. M. Morrell, D.F. Geraghty, S. Honkanen and N. Peyghambarian, "Buried ion-exchanged glass waveguides: burial-depth dependence on waveguide width", Opt. Lett., Vol. 28, No. 13, pp. 1132-1134, 2003.

11. H. Saarikoski, R. P. Salmio, J. Saarinen, T. Eirola and A. Tervonen, "Fast numerical solution of nonlinear diffusion equation for the simulation of ion-exchanged micro-optics components in glass", Opt. Comm., Vol. 134, pp. 362-370, 1997.

12. A. Tervonen, in: S. I. Najafi (Ed.), "Introduction to Glass Integrated Optics", Artech House, Norwood, MA, 1992.

13. D. W. Peaceman and H. H. Rachford, Jr., "The numerical solution of parabolic and elliptic differential equations", J. Soc. Indust. Appl. Math., Vol. 3, pp. 28-41, 1955.

14. L. Palchetti, E. Giorgetti, D. Grando and S. Sottini, "Efficient coupling between annealed K^+-Na^+ Ion-exchanged channel waveguides and 10/125 single-mode fibers at λ=1.321 μm", IEEE J. Quantum Electron., Vol. 34, No. 1, pp.179-189, 1998.

15. D. Marcuse, "Light Transmission Optics", New York: Van Nostrand Reinhold Company, 1972.

16. L. B. Soldano and E. C. M. Pennings, "Optical multi-mode interference devices based on self-imaging: Principles and applications", J. Lightwave Technol. Vol. 13, No. 4, pp. 615-627, 1995.